Contactless Arrhythmia Detection and Short-term HRV Analysis Based on a Fiber Optic Sensor

Weimin Lyu, Tianyu Chen, Shuyang Chen, Weihao Yuan, Yujian Li, Qing Wang, and Changyuan Yu, *Senior Member, IEEE*

***Abstract*—Accurate detection of premature atrial contractions (PACs) is crucial for identifying life-threatening arrhythmias. Traditional electrocardiogram (ECG) devices, which require electrodes attached to the body, often cause discomfort and are unsuitable for long-term monitoring. This paper presents a non-contact ballistocardiogram (BCG) monitoring system utilizing a fiber optic sensor (FOS) for PAC identification and short-term heart rate variability (HRV) analysis. The system employs a Mach-Zehnder interferometer (MZI), which is simple and easy to replicate, consisting of only a 1×2 coupler and a 3×3 coupler. Tiny body vibrations caused by breathing and heartbeats lead to changes in the intensity of the interference light. By detecting these changes using three photodetectors (PDs), vital sign signals can be captured. To evaluate the robustness of the PAC detection algorithm, the study introduced fixed-speed breathing at two respiratory frequencies, increasing the range of interbeat interval (IBI) variations. The correlation coefficient between BCG-derived IBI and ECG-derived IBI in subjects with PAC was 0.9475. The proposed algorithm achieved an accuracy of 94.84% in PAC detection. Additionally, the time-domain and frequency-domain results of BCG-derived HRV and ECG-derived HRV showed high correlation at respiratory rates of 6 beats per minute (bpm) and 15 bpm. The FOS-based BCG signal not only accurately identifies PACs but also facilitates HRV analysis. This proposed system is suitable for long-term, non-contact vital sign monitoring in daily life.**

***Index Terms*—Ballistocardiogram, premature atrial contractions, fiber optic sensor, 3×3 coupler demodulation scheme, heart rate variability**

I. INTRODUCTION

THE cardiovascular disease (CVD) is the leading single cause of death in developed countries, accounting for more than 30% of all deaths in most countries. The American Heart Association (AHA) reports that CVD was responsible for approximately 19.05 million deaths worldwide in 2020. Additionally, one in three people die from cardiovascular-related diseases [1]. Therefore, detecting CVD and finding the underlying causes of its onset for prevention and treatment is crucial. Premature atrial contraction (PAC) is a common cardiac arrhythmia characterized by premature contractions originating in the atria [2]. Normally, the sinus node regulates the heartbeat during normal sinus rhythm, but PAC occurs when another region of the atrium depolarizes before the sinus node. It is often completely asymptomatic and can only be detected by Holter monitoring. PAC occurs in many healthy people and rarely causes symptoms. However, in some cases, PAC may induce more severe arrhythmias, such as atrial flutter or atrial fibrillation (AF), in patients with other underlying structural heart problems [3]. Heart rate variability (HRV) is a specific quantitative indicator of cardiac autonomic regulation [4-6]. This variation reflects autonomic nervous system (ANS) activity, which contains sympathetic nerve system (SNS) and parasympathetic nerve systems (PNS) [7]. Time domain and frequency domain indexes are of great value in predicting heart health. HRV is usually obtained by calculating the changes in consecutive time intervals between QRS complexes of electrocardiogram (ECG) signal [8]. Generally, the HRV index decreases with declining health status.

ECG is one of the non-invasive diagnostic tools commonly used in clinical practice. It is a comprehensive manifestation of the electrical activity of the heart. The heart rate (HR) rhythm can reflect physiological and pathological information and objectively reflect the physiological conditions of various parts of the heart to a certain extent. The ECG characteristic wave can reflect information on the physiological status of the heart. Through the analysis of its shape, amplitude, and duration, it can be used to assist in the diagnosis of CVDs [9]. ECG is the main basis for diagnosing arrhythmia. The HR condition can be identified by continuously monitoring the ECG signal to determine whether an arrhythmia occurs. The traditional arrhythmia diagnosis method is to observe and identify arrhythmia characteristic signals in ECG manually. This process requires long-term observation by the detector. However, obtaining ECG signals requires attaching multiple electrodes to the body, which can cause discomfort to the patient and prevent long-term monitoring [10]. In order to alleviate patients' discomfort during vital signs monitoring, there is an urgent need to study non-contact vital signs monitoring devices to obtain physiological signals

"This work was supported in part by the National Natural Science Foundation of China (Grant No. 62401257) and in part by The Hong Kong Polytechnic University under Grant HKPU 1-WZ01 and HKPU 1-CD8N. *(Corresponding author: Changyuan Yu)*.

W. Lyu, T. Chen, Y. Li, Q. Wang and C. Yu are with Photonics Research Institute, Department of Electrical and Electronic Engineering, The Hong Kong Polytechnic University, Kowloon, Hong Kong (e-mail: weimin.lyu@connect.polyu.hk, tianyu.chen@connect.polyu.hk, yujianwy.li@connect.polyu.hk, wangqing09632629@163.com, changyuan.yu@polyu.edu.hk).

S. Chen is with the Center for Smart Health, School of Nursing, The Hong Kong Polytechnic University, Kowloon, Hong Kong (e-mail: shu-yang.chen@connect.polyu.hk).

Weihao Yuan is with National Key Laboratory of Microwave Photonics, Nanjing University of Aeronautics and Astronautics, Nanjing 211106, China (email: weihao.yuan@nuaa.edu.cn)

conveniently.

The ballistocardiography (BCG) signal reflects the subtle vibrations of the human body caused by each heartbeat and can be obtained in a non-contact method through highly sensitive sensors. In 2006, Alametsä et al. recorded BCG signals with an electromechanical thin film (EMFi) sensor and assessed the severity of breathing disturbances during sleep [11]. Subsequently, in 2011, Wiard et al. used a modified bathroom scale to measure BCG and improve the signal-to-noise ratio (SNR) [12]. In 2017, Hassan et al. proposed a camera-based robust BCG system by measuring head movement [13]. More recently, Escobedo et al. developed a BCG monitoring system using passive radio frequency identification (RFID) technology for HR, RR, and activity identification of individuals on mattresses. The system measures BCG using inductive coupling between an actively powered board and a passive flexible sensing board spaced 3 cm apart [14]. However, the above sensors have some limitations. Scale-based BCG monitoring system requires the patient to remain standing, which is not easy for patients to measure over a long period of time. EMFi-based sensors have low measurement accuracy and require complex circuit design and data processing to improve their SNR. There are privacy concerns with camera-based measurements. Compared with them, Mach–Zehnder interferometer (MZI)-based fiber optic sensor (FOS) has high sensitivity and can accurately detect small vibrations of the body [15,16]. Furthermore, it does not require physical contact and can be used for long periods of time while maintaining user comfort.

While most prior research on PAC detection has focused on ECG-based methods, BCG-based approaches are still emerging and primarily target heartbeat or heart rate detection rather than specific arrhythmias like PAC [17-20]. Ladrova et al. developed a multichannel BCG system and achieved >95% sensitivity in heart rate detection by comparing J-wave detection with ECG references [21]. However, their work did not address arrhythmia classification. Jurčić et al. explored BCG-based heartbeat detection using continuous wavelet transform (CWT), showing improved accuracy in J-peak detection compared to time-domain methods [22]. Again, their focus was on beat detection, not PAC classification. In contrast, our study directly addresses PAC detection using BCG signals, which remains a relatively underexplored area. Our previous work has demonstrated that fiber optic sensors can stably analyze HRV in healthy individuals [23]. The HR of healthy individuals usually shows regularity, and the difference of a few milliseconds between the RR interval and the JJ interval has minimal impact on the results of HRV analysis. However, abnormal heartbeats in PAC patients can lead to transient HR mutations that significantly affect BCG-derived HRV results. Therefore, the feasibility of BCG signal for HRV analysis in PAC patients needs to be further studied. In addition, since different breathing frequencies have great differences in the impact of heartbeat intervals, the subjects performed two different breathing rates of 6 bpm and 15 bpm to verify whether rapid changes in HR affect the accuracy of BCG-based HRV analysis. Our method demonstrates its potential as a non-invasive and unobtrusive alternative to ECG-based systems.

This paper is an extension of our previously published conference paper, where we have significantly expanded the dataset, enhanced the heart rate variability analysis, and introduced new methodologies, such as the LSTM algorithm, to improve the detection and classification of arrhythmias [24]. The experiment uses the signal of commercial ECG equipment as the gold standard, and professionals mark the PAC signal. FOS acquires BCG signals, and the signals are sliced for PAC identification. The R peaks and J peaks of the ECG and BCG signals are respectively used to analyze the corresponding HRV information. The exponential correlations of ECG-derived HRV and BCG-derived HRV were compared in the time domain (SDSD, SDNN, RMSSD, and pNN50) and frequency domain (VLF, LF, HF, and LF/HF ratio). The comparison results of the two signals were used to explore whether the FOS-based BCG signal can be used as a substitute for the traditional ECG signal for arrhythmia identification and short-term HRV analysis in PAC patients. Compared to the gold standard ECG, our system demonstrates promising accuracy in HRV analysis and PAC detection. However, ECG remains superior in terms of signal specificity and established clinical validation. Our system's key advantages lie in its non-contact nature, ease of integration into everyday environments, and potential for long-term, unobtrusive monitoring without the need for electrodes or skin contact.

II. EXPERIMENT

A. System setup

The ECG and BCG signals of PAC patients were acquired using the AD8232 module and FOS, respectively, and recorded via a National Instruments USB-6210 data acquisition card at a sampling rate of 1000 Hz, which ensures accurate signal capture and prevents aliasing in accordance with the Nyquist theorem. The ECG signal is the gold standard for calculating the reference interbeat interval (IBI). Fig. 1 shows the system setup. Fig. 1(a) shows the experimental environment for PAC subjects. The subject sat on the seat, and the FOS was placed under the cushion to collect BCG signals. ECG signals are collected by three electrodes attached to the body. To mitigate motion artifacts in BCG signal acquisition, several methods were employed in this work. The FOS were securely attached and encapsulated with AB glue to ensure long-term stability of the sensing performance. When the subjects sit in a chair, they lean against the backrest for support, maintaining body stability. FOS was placed in areas less affected by respiratory movements, such as inside the seat cushion, to limit exaggerated motion signals caused by chest expansion and contraction during paced respiration. Additionally, a bandpass filter was applied to the BCG waveform, which typically has energy in the range of 1-40 Hz. This filtering attenuates low-frequency components (respiratory components) and high-frequency noise, preserving the most significant BCG content while

suppressing most of the motion artifacts caused by respiration.

Fig. 1(b) shows the main components of the multi-modalities signal acquisition circuit. The 1550nm distributed feedback (DFB) laser with 2mW power is used as the light source, the 3 photodetectors (PDs) are used to receive the 3 output signals of the 2×3 coupler, the MCU (Jetson AGX Orin) is used to demodulate the three signals to eliminate the signal fading problem of the interferometer, the AD8232 module is used to collect the ECG signal, and the onboard Wi-Fi module is used to send the signal to the computer. Fig. 1(c) shows the FOS structure and the connection between FOS and the circuit. A 1×2 coupler and a 2×3 coupler are spliced by a fiber optic fusion splicer to form an MZI and fixed on an acrylic plate with glue to improve the stability of the FOS. Fig. 1(d) shows the typical waveforms of ECG and BCG, and the calculated HR results can be directly viewed on the computer monitor. All data are stored on the computer and processed for PAC identification and HRV analysis.

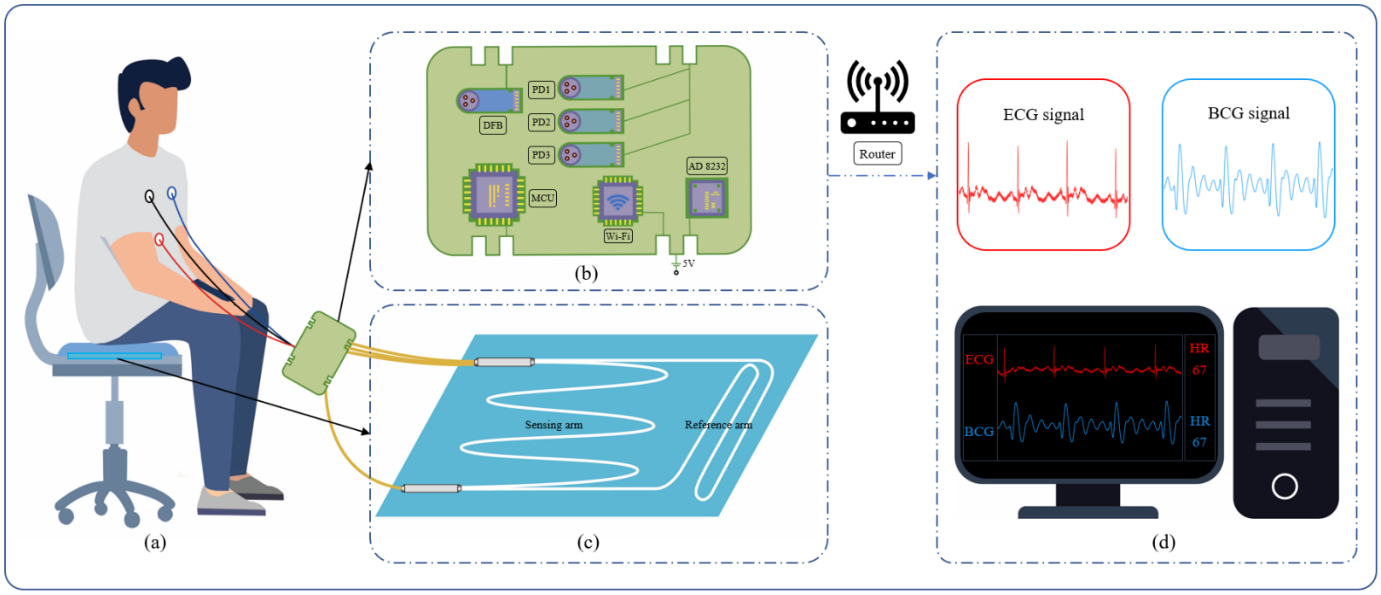

Fig. 1. (a) Experiment setup; (b) multi-modalities signal acquisition circuit; (c) MZI-based FOS structure; (d) ECG-derived and BCG-derived HR results.

The MZI is a highly sensitive optical configuration capable of detecting minute phase shifts caused by physiological micro-vibrations, such as those induced by cardiac and respiratory activity. In a typical MZI, a coherent light source is split into two arms. These beams traverse different optical paths and are then recombined to produce an interference pattern. The resulting optical intensity at the output is governed by the phase difference $\varphi(t)$ between the two arms. Then, the interference light is divided into three outputs with a phase difference of 120°, received by 3 connected PDs. The tiny vibrations of the body caused by the heartbeat will cause a phase difference in the light beams passing through the two arms of the MZI. The intensity of the output lights will also change accordingly. The output light intensity can be expressed as:

$$I_k = D + I_0 \cos[\varphi(t) - (k-1)(2\pi/3)], \quad (1)$$

where $\varphi(t)$ is the phase difference of two light beams, D is the average value of output light intensity, I_0 is the peak intensity of interference fringes, k is the number of the output lights, and $k = 1, 2, 3$.

Here, $\varphi(t)$ is sensitive to changes in optical path length, which can be caused by mechanical vibrations, pressure changes, or refractive index variations due to physiological activity. Fig. 2 shows the adverse effects of MZI bias point variations on the BCG signal. For optimal sensitivity, the MZI is biased at the quadrature point (Q-point), where the slope of the intensity–phase curve is maximal. This ensures a linear relationship between phase variation and output intensity, which is crucial for accurate signal demodulation and physiological parameter extraction.

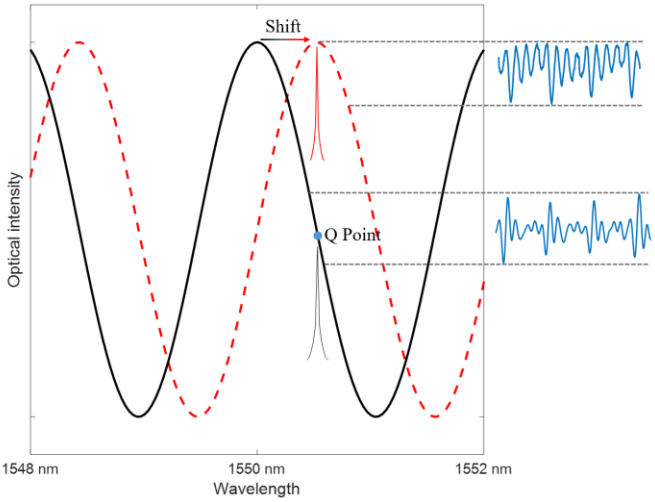

Fig. 2. The effects of MZI bias point change on BCG signal.

However, environmental perturbations (e.g., temperature fluctuations, mechanical stress) can cause the operating point to drift away from the Q-point. When this occurs, the system operates in a nonlinear region of the phase response curve,

leading to signal distortion. This distortion affects the morphology of the BCG waveform, particularly the I, J, and K waves, which are essential for accurate cardiovascular assessment. Therefore, maintaining the operating point at or near the Q-point is therefore critical for reliable physiological monitoring. In this manuscript, a 3×3 coupler demodulation scheme is used to keep the MZI operating point at the Q point.

B. Data collection and processing

All subjects signed an informed consent form before data collection. During the paced respiration experiment, subjects with PAC sat in a chair in a natural posture. They were asked to breathe at fixed rates of 6 bpm and 15 bpm. The two respiration frequencies will cause different changes in the cardiac autonomic rhythm. In particular, there will be obvious changes in IBIs. HRV tends to be higher at lower respiratory rates. This is because slower breathing rates enhance parasympathetic activity, which is associated with increased HRV. At a respiratory rate of approximately 6 bpm, RSA reaches its maximum, leading to greater fluctuations in the intervals between heartbeats. These larger intervals caused by respiration can potentially lead to misidentification of PACs. Therefore, 6 bpm was choosen as one of the controlled breathing rates in this study. As the RR increases, RSA gradually decreases. Consequently, we selected 15 bpm, which is significantly different from 6 bpm, as another controlled RR for comparison. Varying RR beyond these tested values could introduce additional complexities. Faster or slower RR may modulate the HR and the amplitude of the ECG signal differently, potentially introducing more noise or artifacts. This can complicate the signal separation process and reduce the clarity of the PAC signal, leading to potential misdetections. The subjects maintained a fixed rate for 5 minutes of paced respiration, and the FOS and AD8232 modules recorded simultaneously. The recording of each respiratory rate was repeated 5 times, with an interval of 2 minutes for recovery to normal. Infinite impulse response (IIR) bandpass filters with cutoff frequencies of 0.7 and 30 Hz were used to remove high-frequency noise and respiratory signals from BCG and ECG signals. Fig. 3(a) shows a healthy subject's 15-second resting ECG and BCG records. Fig. 3(b) shows a 15-second resting ECG and BCG records of a subject with PAC, and the abnormal heartbeats are circled.

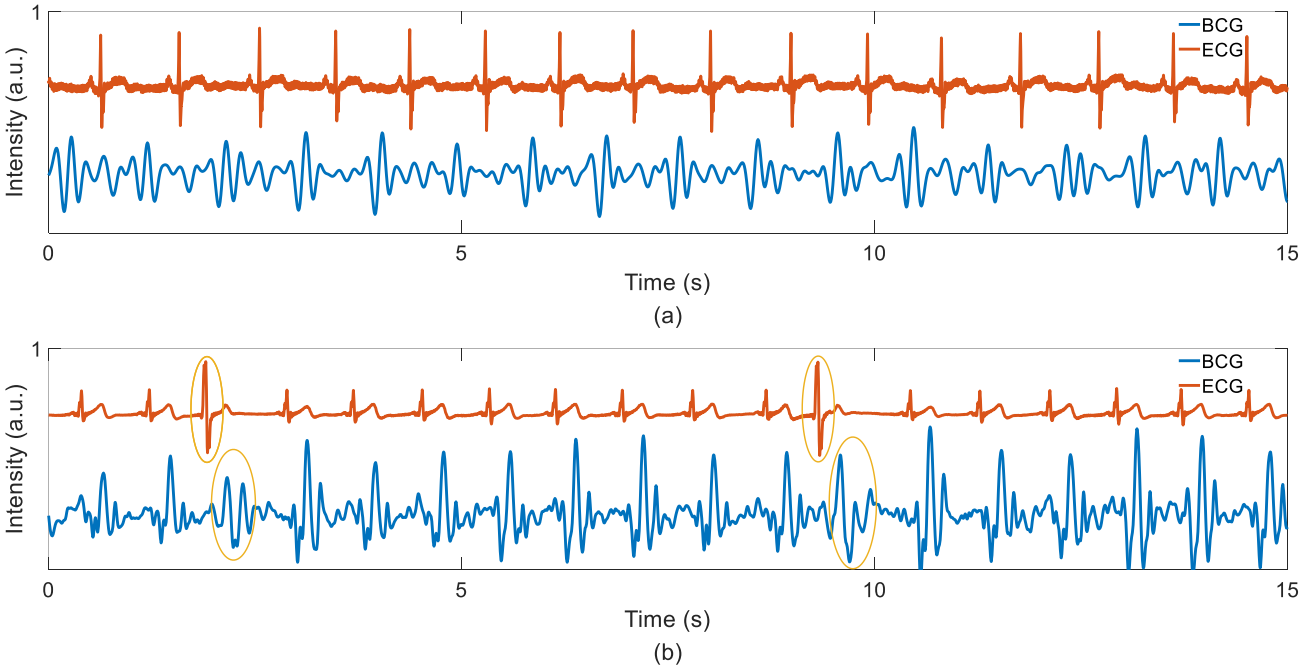

Fig. 3. A 15-second resting ECG and BCG records of (a) a healthy subject and (b) a subject with PAC.

III. RESULTS AND DISCUSSION

The typical ECG and BCG waveforms and the time interval between the two signals are shown in Fig. 4. The main complexes of the two signals are marked in the figure. The QRS complex is the most obvious part of the ECG, corresponding to the depolarization of the left and right ventricles of the heart and the contraction of the large ventricular muscles [25]. It usually lasts 80 to 100 milliseconds. The R wave is often used as a marker for HR calculation, and ECG-derived IBIs can be obtained by calculating the R-R intervals in every two consecutive heartbeats. The most obvious characteristic wave of BCG is called the IJK complex, which corresponds to ventricular

contraction. The J waves are usually the highest amplitude wave in the BCG signal, corresponding to the R waves in the ECG signal [26]. The J-J intervals are commonly used to calculate BCG-derived IBIs. The correlation coefficient between BCG-derived IBIs and the ECG-derived IBIs of subjects with PAC was 0.9475.

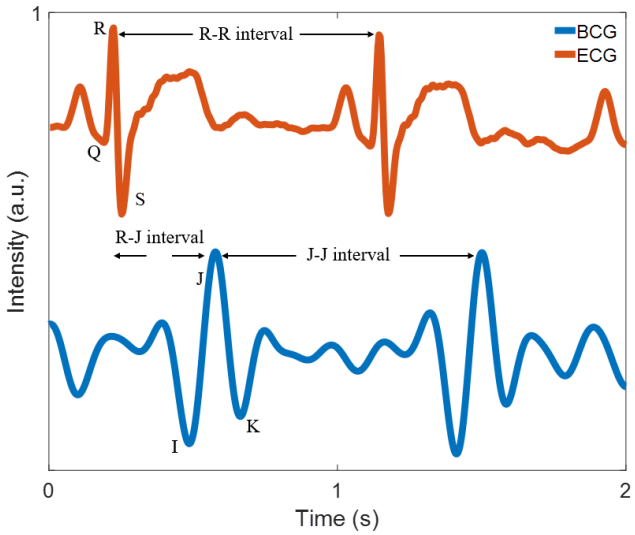

Fig. 4. Typical ECG and BCG waveforms and the time interval between the two signals.

The HR of a healthy adult is 60 to 100 bpm. However, the HR is not always constant and changes with breathing. Because the tension of the vagus nerve and sympathetic nerve changes during breathing, the autonomic rhythm of the sinoatrial node also changes periodically and regularly. The sympathetic nerve tone increases during inhalation, and the HR increases, while the vagal nerve tone increases during expiration, and the HR slows down. The cycle of changes in HR is exactly equal to one breathing cycle, and the HR becomes regular when holding the breath. When the respiratory rate reaches 6 bpm, behavioral relaxation and baroreflex resonance effects are achieved, maximizing HRV. It calms the sympathetic nervous by stimulating the vagus nerve, thereby maximizing the range of heart rate changes during a breathing cycle. In this experiment, two different frequencies of paced respiration (6 bpm and 15 bpm) were introduced to change the IBI. Large changes in IBI will increase the difficulty of identifying PAC. In particular, when the respiratory rate is 6 bpm, the HR change within one respiratory cycle reaches the maximum [24]. The R-J intervals are the time difference between the R waves of the ECG signal and the J waves of the BCG signal, reflecting the time intervals between ventricular depolarizations and contractions [27]. The intervals will vary based on the individual's cardiac conditions, which can be altered through exercise and the Valsalva maneuver. It also rises and falls with paced respiration, which results in acceptable deviations between BCG-derived IBIs and ECG-derived IBIs.

A. PAC detection

Each recording was for 5 minutes, and motion artifacts were removed by previous algorithms [28]. The clean signal is sliced into 4-second segments. After the sliding window division, we will get several 1000-dimensional vectors as inputs to the deep neural network. The labeling of each sliding window was experimentally verified. When a premature BCG signal appears in a window, the entire window will be classified as a premature signal window and assigned label 1. Conversely, for a window where only normal BCG signals exist, label 2 will be used. Fig. 5 shows the structure of the complete deep neural network used in this work.

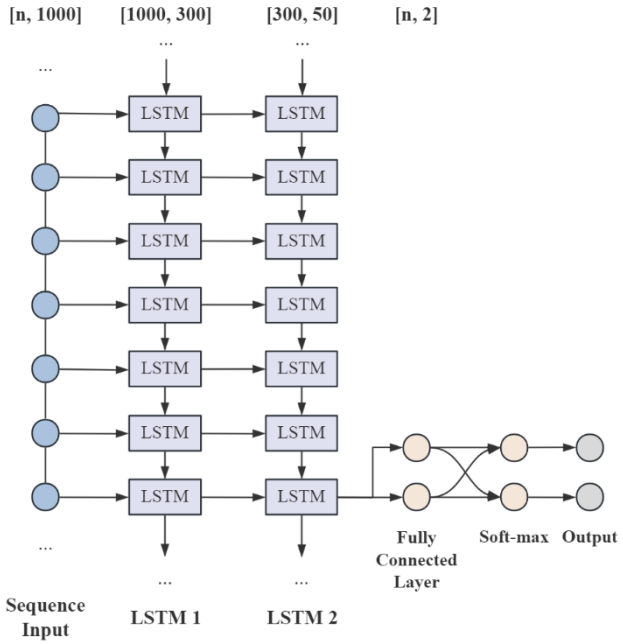

Fig. 5. Structure of deep neural network.

LSTM networks exhibit remarkable advantages in handling sequential data. Their unique architecture, including forget gates, input gates, and output gates, allows them to effectively capture and leverage long-term dependencies in temporal sequences. Compared to traditional recurrent neural networks (RNNs), LSTMs are more adept at addressing the issues of vanishing or exploding gradients and can maintain information from input sequences over extended periods. This makes them particularly effective for tasks such as language modeling, machine translation, and time series prediction. Specifically, when dealing with long sequences or scenarios with extended dependencies, LSTMs accurately identify patterns and regularities within the sequence [29]. An LSTM-based neural network structure will be implemented to distinguish normal BCG signals from premature beats accurately. This structure includes a sequence input layer, followed by two LSTM layers interspersed with rectified linear unit (ReLU) activation layers. Each window will serve as input to the neural network, providing a continuous 4000-dimensional time series signal. The first LSTM layer contains 300 units and operates in sequence output mode, preserving temporal information throughout the sequence. A ReLU activation layer then introduces non-linearity before feeding into the second

LSTM layer, which has 50 units and produces a single output corresponding to the last time step. A fully connected layer with two output units is used for classification, followed by a soft-max layer to compute class probabilities. The Adam optimization algorithm supports the training process with a mini-batch size of 50. The maximum number of epochs is 50, with an initial learning rate of 0.0001. A piecewise learning rate schedule is used, where the learning rate decreases by 0.01 after every 300 epochs. Data shuffling is performed at each epoch to improve training robustness. Simple cross-validation was employed, where the dataset was divided into 70% for the training set and 30% for the testing set. The model was trained on the training set and evaluated on the testing set. This process was repeated multiple times with different data splits.

Fig. 6 shows the confusion matrix of the test set in the PAC detection task. The accuracy of the proposed algorithm in the PAC detection task is 94.8424%. Fig. 7 shows the ROC curve for test data. The detailed performance of the confusion matrix is shown in Table I.

Fig. 6. Confusion matrix of the test set of subjects with PAC.

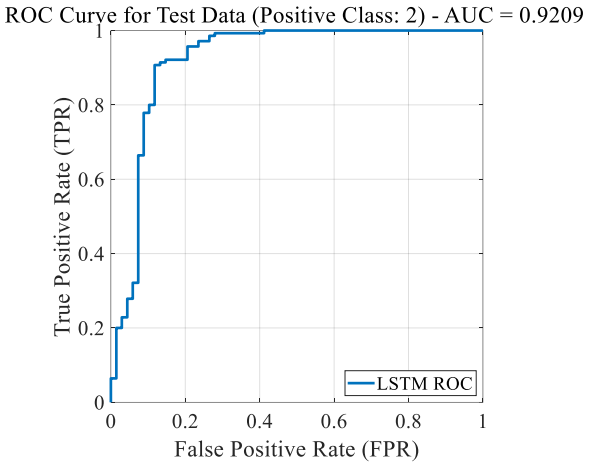

Fig. 7. ROC curve for test data.

TABLE I
PERFORMANCE OF THE CONFUSION MATRIX

Metric	Normal Class (%)	PAC Class (%)
Recall	99.4	89.9
Precision	90.8	99.3
F1-Score	94.9	94.4
TPR	94.9	94.4
FPR	10.1	0.6

B. HRV time-domain analysis

Time-domain HRV reflects autonomic homeostasis, which is essential for assessing an individual's psychological and metabolic health [30]. Time domain HRV refers to numbers obtained from statistical analysis of the intervals between heartbeats. Table II shows the commonly used time domain HRV indexes [31]. SDNN is the standard deviation of the N-N intervals, which reflects the total HRV for a period of interest. It correlates more with SNS activity and the total power band than with the HF band. Therefore, the contribution of the LF band to the generation of SDNN is greater than that of the HF band. It is considered the gold standard for predicting cardiovascular risk. To obtain the RMSSD, calculate each consecutive time difference (in milliseconds) between heartbeats. Then, square each value and average the results to get the square root of the sum. It is the primary time-domain HRV index of PNS activity and highly correlates with high-frequency power [32]. It is not affected by RSA and is the most important HRV parameter in the elderly population. SDSD is the standard deviation of the difference between adjacent R-R intervals. pNN50 is the percent of successive differences of intervals between heartbeats greater than 50ms. It is correlated to the RMSSD and HF power and reflects the PNS activity. These indexes are key parameters of HRV and can be used to evaluate cardiovascular health, stress levels, emotional state, and exercise recovery.

TABLE II
HRV TIME DOMAIN INDEXES

Index	Definition
SDNN	Standard deviation of all N-N intervals
RMSSD	Square root of the mean of the sum of the squares of differences between adjacent N-N intervals
SDSD	Standard deviation of differences between adjacent N-N intervals
pNN50	Percent of difference between adjacent N-N intervals that are greater than 50ms

N-N: the interval between two adjacent heartbeats.

Fig. 7 shows the ECG-derived and BCG-derived HRV signals for PAC subjects under paced respiration at 6 bpm and 15 bpm, respectively. Since the respiratory rate of 6 bpm will lead to a larger HRV amplitude, the values of time domain indexes at this respiratory rate will be greater than those at the respiratory rate of 15 bpm. As mentioned earlier, paced respiration will change the hemodynamic status, resulting in changes in the R-J interval [33]. Therefore, there are certain

errors in the time domain indexes calculated by the R-R intervals and J-J intervals. The results in Fig. 8 show acceptable deviations for all time domain indexes at both breathing rates.

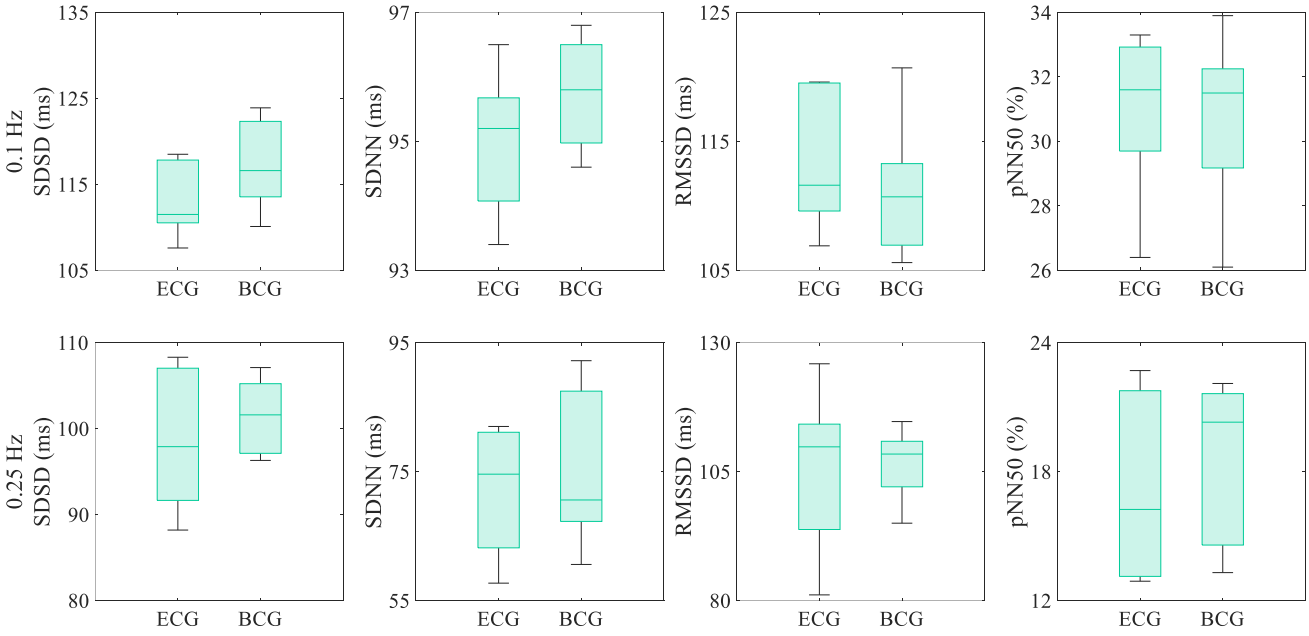

Fig. 8. BCG and ECG HRV time-domain indexes at 6 bpm (top) and 15 bpm paced respiration (bottom).

C. HRV frequency-domain analysis

HRV is analyzed in the frequency domain by counting the number of N-N intervals that match each specific frequency band. These frequency bands are very low frequency (VLF) band from 0.0033 to 0.04 Hz, low frequency (LF) band from 0.04 to 0.15 Hz, and high frequency (HF) band from 0.15 to 0.4 Hz [34]. Since the ultra low frequency (ULF) band reflecting circadian and neuroendocrine is not meaningful for short-term HRV recordings, this frequency band is not analyzed in this study [35]. The band ranges are shown in Table III. Although the PAC patients participating in the test try to control the prescribed respiratory rate, there are still some deviations in each respiratory cycle, which will affect the results of the frequency domain analysis. This limitation can be overcome by averaging data from multiple experiments.

TABLE III
HRV FREQUENCY DOMAIN INDEXES

Index	Frequency band (Hz)
VLF	0.0033-0.04
LF	0.04-0.15
HF	0.15-0.4
LF/HF ratio	/

Fig. 9 (a)-(d) depict the HRV PSD of ECG and BCG for a subject with PAC at respiratory rates of 6 bpm and 15 bpm. The total power, which is the sum of HF, LF, and VLF bands produced by the heart, represents the overall autonomic activity, with the sympathetic activity being the main contributor. Lower values typically indicate that the individuals are either exhausted or ill. A higher total power within a reasonable range is preferable. The PSD results of the BCG-derived and ECG-derived HRV at both respiratory rates exhibit similar patterns.

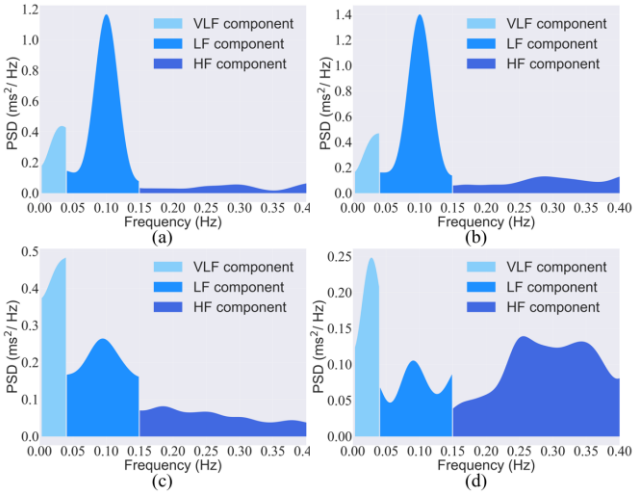

Fig. 9. (a) BCG-derived and (b) ECG-derived HRV PSD of a subject with PAC at 6 bpm paced respiration. (c) BCG-derived and (d) ECG-derived HRV PSD of a subject with PAC at 15 bpm paced respiration.

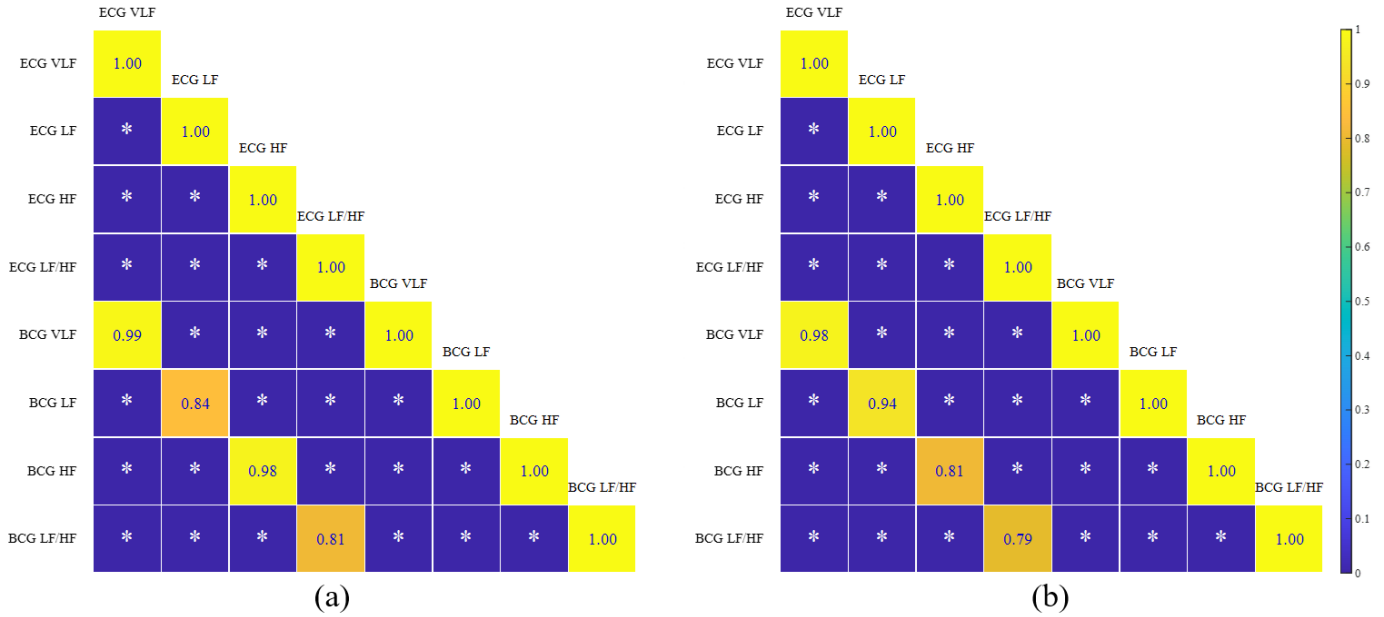

Fig. 10. Frequency domain indexes correlation coefficients between ECG and BCG in PAC subjects during paced respiration at (a) 6 bpm and (b) 15 bpm.

VLF band values fluctuate rapidly, usually within seconds or minutes, and can significantly differ even among continuous measurements [36]. This parameter generally represents the overall activity of various slow sympathetic function mechanisms. A high VLF band value usually suggests stress. When the subject is calm and relaxed, LF band values indicate baroreflex control of sympathetic nerve activity, which is the quickest mechanism for blood pressure regulation. Higher LF band values occur during yawning, inhaling, or breathing at a rate of 6 bpm, indicating increased parasympathetic activity. Fig. 9(a) and (b) show the results for respiratory rates of 6 bpm, where the LF band is the main component of the PSD. The HF band is dependent on parasympathetic activity and respiratory sinus arrhythmia (normal HR changes during inhalation and exhalation). However, as shown in Fig. 9(c) and (d), the LF band component significantly decreases at 15 bpm paced respiration, while the VLF band and HF band components increase at the same rate. The HF band is regulated by the parasympathetic activity of the autonomic nervous system, which is the major determinant of respiratory sinus arrhythmia. An increase in heart rate is typically associated with the activation of the sympathetic nervous system and the inhibition of the parasympathetic nervous system. The LF band reflects the combined activity of both systems, while the HF band primarily reflects parasympathetic activity. As the heart rate increases, the sympathetic influence grows, potentially causing the LF band to decrease, while the rapid adjustments by the parasympathetic system lead to an increase in the HF band. In PAC patients, the heart's electrophysiological characteristics may alter the frequency domain features of HRV. PACs induce abnormal electrical activity in the heart, which can affect HRV frequency domain analysis, leading to an increase in the VLF and HF bands.

HF band values are typically higher at night than during the day. If these values continue to decrease throughout the day, it could indicate chronic stress. The LF/HF ratio represents the overall balance between the SNS and the PNS. Higher values indicate a dominance of the SNS, while lower values indicate a dominance of the PNS.

In addition to PSD analysis, the correlation coefficients of different frequency bands derived from ECG and BCG signals recorded every five minutes were compared to describe the accuracy of BCG-derived HRV. Even though the abnormal heartbeat of PAC patients will cause the change of the RJ interval to be larger than the normal value, it will not have much impact on the correlation of frequency indexes. Fig. 10 shows the correlation coefficient results between ECG-derived and BCG-derived HRV frequency domain indexes during paced respiration in subjects with PAC. The results showed that the BCG-derived HRV frequency distribution at both respiratory frequencies highly correlated with the corresponding ECG-derived HRV frequency distribution. The correlation results of VLF and LF/HF ratio are similar at the two respiratory frequencies. The correlation of the VLF band shows an extremely high correlation at both respiratory frequencies, while the accuracy of LF/HF bands is slightly lower. The correlation results of the LF band and HF band under the two respiratory frequencies are opposite. The correlation of the HF band is higher at the respiratory rate of 6 bpm, and the correlation of the HF band is higher at the respiratory rate of 15 bpm.

D. Limitations

The proposed non-contact BCG monitoring system utilizing a fiber optic sensor demonstrates promising performance in detecting PAC and analyzing HRV, however, several limitations remain. The system is inherently sensitive to

motion artifacts, as external vibrations and body movements can introduce noise that affects the accuracy of PAC detection and HRV analysis. Additionally, although the study reports high correlation and accuracy, the validation is currently limited to specific conditions and a relatively small sample size, necessitating broader testing across diverse populations and environments to confirm its robustness. Furthermore, while the system shows potential, comprehensive comparisons with established ECG-based methods under various scenarios are essential to fully establish its reliability and clinical applicability. Addressing these limitations through future research and development will be crucial for enhancing the system's performance and enabling its use in real-world, long-term, non-contact vital sign monitoring.

IV. CONCLUSION

The FOS-based BCG monitoring system proposed in this study can obtain high-quality BCG signals for PAC detection and short-term HRV analysis. PAC is a premature contraction originating from the atria. In some cases, it can trigger more serious heart arrhythmias such as atrial flutter or AF. Accurate detection of PAC is important for daily health monitoring. In addition, HRV reflects the autonomic function of the heart. Many cardiac and non-cardiac diseases are associated with changes in HRV. The proposed system can stably acquire high-precision BCG signals for HRV analysis over a long period of time. This study identified PAC based on the proposed system and analyzed the short-term HRV accuracy of subjects with PAC. The time domain indexes of BCG-derived HRV and ECG-derived HRV show acceptable deviations, and the frequency domain indexes of BCG-derived HRV and ECG-derived HRV have satisfactory correlation coefficients. The results of this study demonstrate the promise of FOS-based BCG signals as a non-contact measurement method for heart health monitoring.

REFERENCES

[1] C. W. Tsao et al., "Heart disease and stroke statistics–2022 update: A report from the American Heart Association," *Circulation*, vol. 145, no. 8, pp. e153-e639, 2022.

[2] A. Yang et al., "Advanced Pacemaker Diagnostic features in the characterization of atrial fibrillation: impact on preventive pacing algorithms," *Pacing and Clinical Electrophysiology*, vol. 26, no. 1p2, pp. 310-313, 2003.

[3] T. J. Jensen, J. Haarbo, S. M. Pehrson, and B. Thomsen, "Impact of premature atrial contractions in atrial fibrillation," *Pacing and Clinical Electrophysiology*, vol. 27, no. 4, pp. 447-452, 2004.

[4] J. Luo et al., "Quantitative analysis of heart rate variability parameter and mental stress index," *Frontiers in Cardiovascular Medicine*, vol. 9, pp. 930745-930745, 2022.

[5] J. Philip. Sanko and R. E. DeMeersman, "A comparison of power spectral analysis of heart rate variability and blood pressure variability in health, young men and women exposed to a local thermal stress," *Ed.D. thesis,* Columbia University Teachers College, 1996.

[6] U. Rajendra Acharya, K. Paul Joseph, N. Kannathal, C. M. Lim, and J. S. Suri, "Heart rate variability: A review," *Medical & Biological Engineering & Computing*, vol. 44, no. 12, pp. 1031-1051, 2006.

[7] B. Aysin and E. Aysin, "Effect of respiration in heart rate variability (HRV) analysis," in *Proceedings of the 28th Annual International Conference of the IEEE Engineering in Medicine and Biology Society*, vol. 1-15, pp. 1776-1779, 2006.

[8] P. Karthikeyan, M. Murugappan, and S. Yaacob, "Detection of human stress using short-term ECG and HRV signals," *Journal of Mechanics in Medicine and Biology*, vol. 13, no. 2, pp. 1350038, 2013.

[9] J. Jin, "Screening for cardiovascular disease risk with ECG," *JAMA: the Journal of the American Medical Association*, vol. 319, no. 22, pp. 2346, 2018.

[10] K. Arquilla, A. K. Webb, and A. P. Anderson, "Textile electrocardiogram (ECG) electrodes for wearable health monitoring," *Sensors*, vol. 20, no. 4, pp. 1013, 2020.

[11] J. Alametsä et al., "Automatic detection of spiking events in EMFi sheet during sleep," *Medical Engineering & Physics*, vol. 28, no. 3, pp. 267-275, 2006.

[12] R. M. Wiard, O. T. Inan, B. Argyres, M. Etemadi, G. T. A. Kovacs, and L. Giovangrandi, "Automatic detection of motion artifacts in the ballistocardiogram measured on a modified bathroom scale," *Medical & Biological Engineering & Computing*, vol. 49, no. 2, pp. 213-220, 2011.

[13] M. A. Hassan, A. S. Malik, D. Fofi, N. M. Saad, Y. S. Ali, and F. Meriaudeau, "Video-Based Heartbeat Rate Measuring Method Using Ballistocardiography," *IEEE Sensors Journal*, vol. 17, no. 14, pp. 4544-4557, 2017.

[14] P. Escobedo, P. Antonio, L. Nuria, A. C. Miguel, J. P. Alberto, and M. Antonio, "Bed-based ballistocardiography system using flexible RFID sensors for non-invasive single-and dual-subject vital signs monitoring." *IEEE Transactions on Instrumentation and Measurement*, vol. 73, pp. 1-12, 2024.

[15] W. Chen et al., "Non-Invasive Measurement of Vital Signs Based on Seven-Core Fiber Interferometer," *IEEE Sensors Journal*, vol. 21, no. 9, pp. 10703-10710, 2021.

[16] S. Šprager and D. Zazula, "Detection of heartbeat and respiration from optical interferometric signal by using wavelet transform," *Computer Methods and Programs in Biomedicine*, vol. 111, no. 1, pp. 41-51, 2013.

[17] H. Zhang, Z. Wang, C. Teng, S. Kumar, X. Li, and R. Min, "Wearable Cardiorespiratory Sensor for Real-Time Monitoring with Smartphone Integration," *IEEE Transactions on Instrumentation and Measurement*, vol. 73, pp. 1-1, 2024.

[18] H. Cui et al., "Statistical analysis of the consistency of HRV analysis using BCG or pulse wave signals," *Sensors*, vol. 22, no. 6, pp. 2423, 2022.

[19] J. H. Shin, S. H. Hwang, M. H. Chang, and K. S. Park, "Heart rate variability analysis using a ballistocardiogram during valsalva manoeuvre and post exercise," *Physiological Measurement*, vol. 32, no. 8, pp. 1239-1264, 2011.

[20] G. Parchani, G. Kumar, R. Rao, K. Udupa, and V. Saran, "Efficacy of Non-contact BallistocardiographySystem to Determine Heart Rate Variability," *Annals of Neurosciences*, vol. 29, no. 1, pp. 16-20, 2022.

[21] M. Ladrova, F. Barvik, J. Brablik, R. Jaros, and R. Martinek, "Multichannel Ballistocardiography: A Comparative Analysis of Heartbeat Detection Across Different Body Locations," *PloS one*, vol. 19, no. 8, pp. e0306074, 2024.

[22] K. Jurčić, P. R. Zarate, R. Magjarević, E. Pino, and P. de Carvalho, "Heart Rate Detection from Ballistocardiogram Using Continuous Wavelet Transformation," in International Conference on Biomedical and Health Informatics 2022, ICBHI 2022, Switzerland: Springer International Publishing AG, 2024, pp. 305-311.

[23] W. Lyu et al., "Non-contact short-term heart rate variability analysis under paced respiration based on a robust fiber optic sensor system," *IEEE Transactions on Instrumentation and Measurement*, vol. 73, pp. 1-13, 2024.

[24] W. Lyu, S. Chen, W. Yuan, Y. Li, Q. Wang and C. Yu, "Non-contact short-term HRV analysis of patients with premature beats based on a fiber optic sensor," in 28th International Conference on Optical Fiber Sensors (OFS) 2023, pp. Tu4-2, Hamamatsu, Japan, November 20-24, 2023.

[25] D. Hayn, B. Jammerbund, and G. Schreier, "QRS detection based ECG quality assessment," *Physiological Measurement*, vol. 33, no. 9, pp. 1449-1461, 2012.

[26] W. R. Scsrborough and S. A. Talbot, "Proposals for ballistocardiographic nomenclature and conventions: revised and extended report of committee on ballistocardiographic terminology," *Circulation*, vol. 14, no. 3, pp. 435-450, 1956.

[27] J. Alametsä, A. Palomäki, and J. Viik, "Short and longer term repeatability of ballistocardiography in a sitting position with EMFi sensor," *Medical & Biological Engineering & Computing*, vol. 49, no. 8, pp. 881-889, 2011.

[28]S. Chen et al., "Deep Learning-Based Ballistocardiography reconstruction algorithm on the optical fiber sensor," *Optics Express*, vol. 30, no. 8, pp. 13121-13133, 2022.
[29]K. Smagulova and A. P. James, "A survey on LSTM memristive neural network architectures and applications," *The European Physical Journal Special Topics*, vol. 228, no. 10, pp. 2313-2324, 2019.
[30]M. Malik, "Time-domain measurement of heart rate variability," *Cardiac Electrophysiology Review*, vol. 1, no. 3, pp. 329-334, 1997.
[31]F. Wang, K. Sagawa, and H. Inooka, "Time domain heart rate variability index for assessment of dynamic stress," in *Computers in Cardiology*, vol. 25, pp. 97-100, 1998.
[32]F. Shaffer and J. P. Ginsberg, "An overview of heart rate variability metrics and norms," *Frontiers in Public Health*, vol. 5, pp. 258-258, 2017.
[33]W. Lyu, W. Xu, F. Yang, S. Chen, F. Tan, and C. Yu, "Non-invasive measurement for cardiac variations using a fiber optic sensor," *IEEE Photonics Technology Letters*, vol. 33, no. 18, pp. 990-993, 2021.
[34]J. D. Blood et al., "The variable heart: High frequency and very low frequency correlates of depressive symptoms in children and adolescents," *Journal of Affective Disorders*, vol. 186, pp. 119-126, 2015.
[35]M. Yilmaz, H. Kayancicek, and Y. Cekici, "Heart rate variability: Highlights from hidden signals," *Journal of Integrative Cardiology*, vol. 4, no. 5, pp.1-8, 2018.
[36]H. Usui and Y. Nishida, "The very low-frequency band of heart rate variability represents the slow recovery component after a mental stress task," *PloS one*, vol. 12, no. 8, pp. e0182611-e0182611, 2017.